ACS Energy Letters

http://pubs.acs.org/journal/aelccp

LETTER

Superlattices are Greener on the Other Side: How Light Transforms Self-Assembled Mixed Halide Perovskite Nanocrystals

Michael C. Brennan,* Stefano Toso, Ilia M. Pavlovetc, Maksym Zhukovskyi, Sergio Marras, Masaru Kuno,* Liberato Manna,* and Dmitry Baranov*

Cite This: *ACS Energy Lett.* 2020, 5, 1465−1473

Read Online

ACCESS | Metrics & More | Article Recommendations | Supporting Information

ABSTRACT: **Perovskite nanocrystal superlattices (NC SLs) are the nearest real-world approximations to monodisperse NC ensembles. NC SLs thus represent ideal model systems for evaluating the optical and structural stability of $CsPb(I_{1-x}Br_x)_3$ NCs at a macroscopic level. Here, photoinduced changes to $CsPb(I_{1-x}Br_x)_3$ NC SLs ($0 < x < 1.0$) are probed via *in situ* photoluminescence, X-ray diffraction, and electron microscopy. We find that prolonged (~10−20 h) ultraviolet−visible irradiation causes irreversible PL blueshifts, photobrightening, and crystal structure contractions. These changes stem from gradual photoinduced I_2 sublimation, which transforms $CsPb(I_{1-x}Br_x)_3$ into $CsPbBr_3$. Despite eliminating half of the initial halides from individual $CsPb(I_{0.53}Br_{0.47})_3$ particles, NCs within SLs remarkably preserve their initial crystallinity, cuboidal shapes, edge lengths, and size distributions. This work illustrates compositional control toward generating precisely engineered perovskite NC SLs. It also highlights iodide photo-oxidation as a hurdle that must be overcome if mixed halide perovskite nanomaterials are to be applied beyond fundamental studies.**

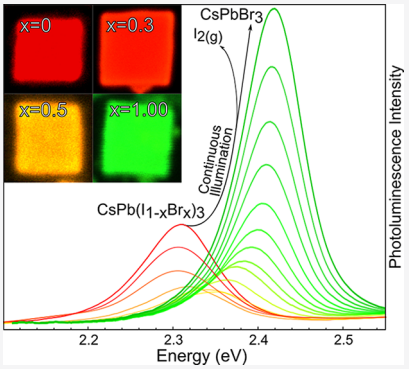

All-inorganic $CsPbX_3$ ($X^- = I^-$, Br^-, Cl^-) perovskite nanocrystals (NCs) embody excellent photoluminescence (PL) properties, which include high PL quantum yields, narrow emission line widths, and fast radiative lifetimes.[1−14] Halide alloying [e.g., $CsPb(I_{1-x}Br_x)_3$] permits precise band gap (E_g) control between ~3.1 eV (400 nm) and ~1.7 eV (730 nm).[1,4−6,15−19] Tunable band gaps and bright, color-specific emission have generated great interest in implementing mixed halide nanomaterials into quantum dot displays as well as multijunction solar cells.[16] These applications require NCs that are stable under prolonged excitation. Unfortunately, the optical and structural properties of mixed halide perovskites are dramatically altered under continuous illumination.

Uniformly mixed halide perovskite thin films ($0.2 < x < 1.0$) are well known[20−24] to undergo reversible segregation into low-E_g I-rich ($x \approx 0.2$) and high-E_g Br-rich domains under continuous wave (CW) visible illumination. Light-induced halide segregation has been established through observations of Bragg reflections splitting into two distinct peaks in X-ray diffraction (XRD) measurements.[24] The lower (higher) angle peak represents the crystal structure expansion (contraction) associated with the formation of I-rich (Br-rich) domains. Favorable band offsets then lead to preferred charge carrier accumulation in I-rich domains. As a direct consequence, photoinduced PL redshifts to energies associated with I-rich $x \approx 0.2$ compositions have been almost universally observed in $APb(I_{1-x}Br_x)_3$ [$A^+ = CH_3NH_3^+$ (MA^+), $CH(NH_2)_2^+$ (FA^+), Cs^+] thin films.[21] The phenomenon is reversible, and in the dark both PL and XRD peaks recover to their initial positions.

In contrast to mixed halide perovskite thin films, there has been significantly less work on photoinduced halide segregation in mixed halide perovskite NCs. Complicating the issue are disparate reports in the literature regarding the photostability of mixed halide perovskites at the nanometer scale. Draguta et al.[22] first demonstrated that colloidal $CsPb(I_{0.50}Br_{0.50})_3$ NC films (average NC edge length, $l \approx 10$ nm) are stable under CW illumination conditions (excitation wavelength, $\lambda_{exc} = 405$ nm; excitation intensity, $I_{exc} = 40$ mW cm^{-2}, ~2 min exposure) that induce halide segregation in analogous $CsPb(I_{0.50}Br_{0.50})_3$ and $MAPb(I_{0.50}Br_{0.50})_3$ thin films. The improved NC photostability against halide segregation

Received: March 20, 2020
Accepted: April 6, 2020
Published: April 6, 2020

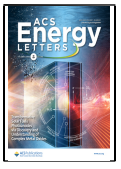

https://dx.doi.org/10.1021/acsenergylett.0c00630
ACS Energy Lett. 2020, 5, 1465−1473

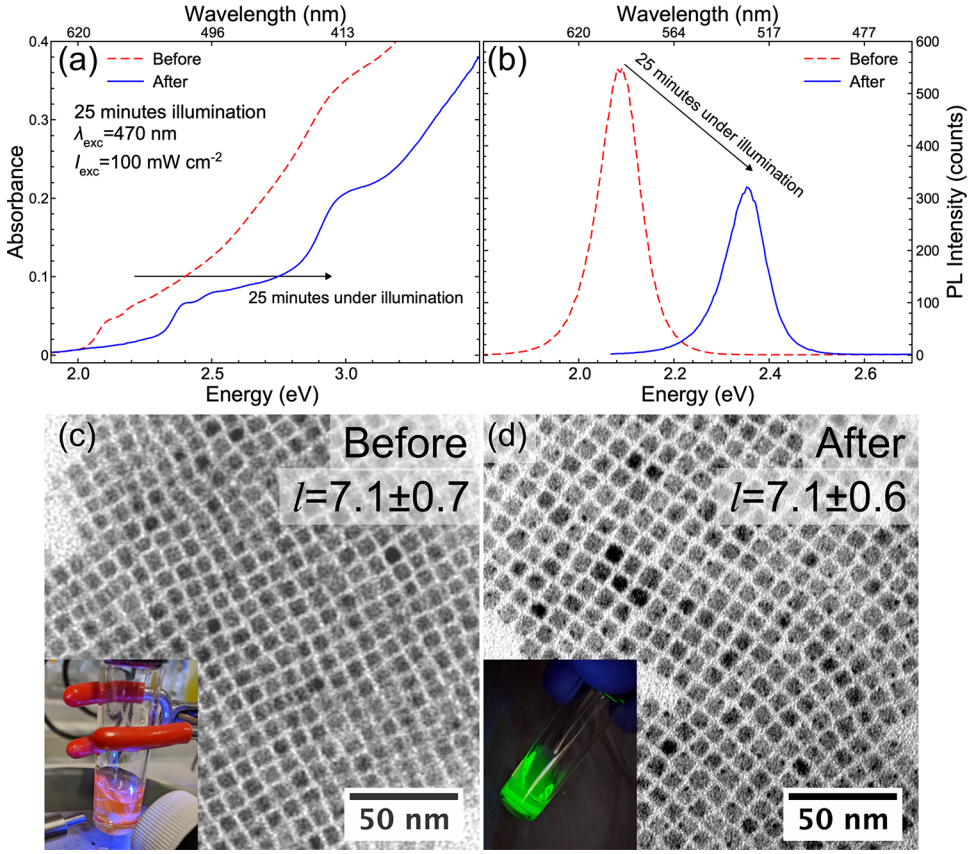

Figure 1. (a) Absorption and (b) PL spectra of $CsPb(I_{0.64}Br_{0.36})_3$ NCs in toluene before (dashed red lines) and after (solid blue lines) 25 min of CW illumination (LED source, λ_{exc} = 470 nm; I_{exc} = 100 mW cm^{-2}). TEM images of mixed halide x = 0.36 NCs before (c) and after (d) CW illumination. Insets in panels c and d show photographs of the visible PL of $CsPb(I_{0.64}Br_{0.36})_3$ NCs in toluene before and after the illumination experiment, respectively.

was linked to limited carrier diffusion lengths at small sizes. This concept underlies a model for light-induced halide segregation in mixed halide perovskite thin films.[22] Gualdrón-Reyes et al.[25] subsequently corroborated these results, showing that $CsPb(I_{1-x}Br_x)_3$ NC films (x = 0.11, 0.52, and 0.79) are stable under CW illumination (λ_{exc} = 405 nm; I_{exc} = 10 mW cm^{-2}, ~10 min exposure) when l < 45 nm.

At higher excitation intensities, however, both emission redshifts and blueshifts have been reported. Here, Draguta et al.[22] have observed the emergence of I-rich emission at ~1.80 eV after 20 s of I_{exc} = 500 W cm^{-2} CW illumination (λ_{exc} = 405 nm) in $CsPb(I_{0.5}Br_{0.5})_3$ NC films. Wang et al.[26] also reported red-shifted I-rich emission at ~1.87 eV in $CsPb(I_{1-x}Br_x)_3$ NC films ($l \approx$ 35 nm, x = 0.7, 0.6, 0.5, 0.4) following 10 min of I_{exc} = 300 mW cm^{-2} CW illumination (λ_{exc} = 405 nm). In contrast to these above-mentioned studies, Zhang et al.[27] reported that close-packed $CsPb(I_{0.60}Br_{0.40})_3$ NC films and individual NCs blueshift to ~2.4 eV under ~50 min of quasi-CW illumination (λ_{exc} = 405 nm; I_{exc} > 30 W cm^{-2}). These divergent observations highlight the need for further investigations of photoinduced transformations in mixed halide perovskite NCs.

To date, light-induced changes to $CsPb(I_{1-x}Br_x)_3$ NCs have primarily been studied via PL-based techniques.[21,25−27] This prompts questions as to how illumination alters the NCs' shapes, sizes, size distributions, and crystal structures. Here, we perform a comprehensive optical and structural analysis of the light-induced changes to $CsPb(I_{1-x}Br_x)_3$ NC superlattices (SLs). Mixed halide NC SLs represent shape- and size-pure forms of NC ensembles. They are, therefore, ideal specimens for revealing changes to the structural and optical properties of mixed halide NCs in close-packed films under illumination. Beyond this, perovskite NC SLs offer tantalizing opportunities for realizing collective, macroscopic quantum phenomena, as evidenced by recent reports of cooperative effects from individual $CsPbBr_3$ NC SLs.[28−37]

In what follows, we demonstrate the existence of photoinduced changes to $CsPb(I_{1-x}Br_x)_3$ NCs within NC SLs. Specifically, we observe light-induced changes to the stoichiometry of mixed halide NCs that stem not from anion segregation, but rather from photoinduced I_2 sublimation. In effect, a light-induced $CsPb(I_{1-x}Br_x)_3$ to $CsPbBr_3$ transformation occurs with concomitant changes to NC structure and optical response. More intriguingly, the photoconversion of NC SLs is shape-preserving, pointing to the structural stability of cation substructure despite losses of nearly half of the anions initially present in component NCs.

Photoinduced Transformation of Mixed Halide $CsPb(I_{1-x}Br_x)_3$ NCs in Solution. Figure 1 first illustrates the impact that 25 min of CW illumination (LED source, λ_{exc} = 470 nm; I_{exc} = 100 mW cm^{-2}) has on a dilute dispersion of $CsPb(I_{1-x}Br_x)_3$ NCs (x = 0.36, l = 7.1 ± 0.7 nm) in toluene. Under photoexcitation, the specimen's visually bright orange PL changes to green with nearly a complete loss of intensity (Supporting Information Figure S1). The PL partially recovers a few minutes after the CW illumination is switched off (see Figure S2). Strikingly, significant shifts to higher energy exist in both absorption

https://dx.doi.org/10.1021/acsenergylett.0c00630
ACS Energy Lett. 2020, 5, 1465−1473

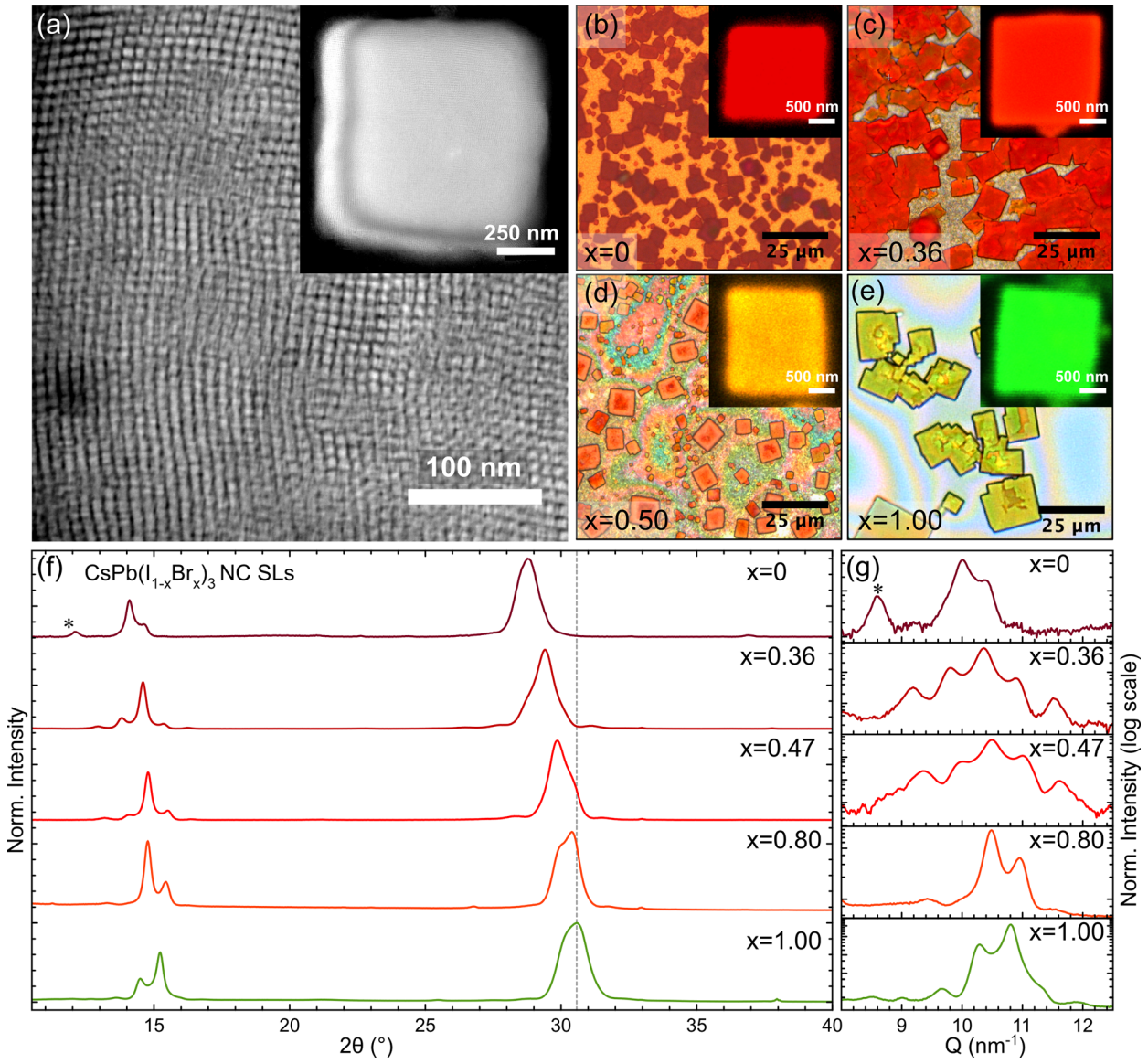

Figure 2. (a) HAADF-STEM image of NCs within a $CsPb(I_{0.50}Br_{0.50})_3$ NC SL. Inset: HAADF-STEM image of an entire $x = 0.50$ NC SL. Optical microscopy images of $CsPb(I_{1-x}Br_x)_3$ SLs for (b) $x = 0$, (c) $x = 0.36$, (d) $x = 0.50$ and (e) $x = 1.00$ (e). Insets of each optical image are the associated spatially resolved PL maps of individual NC SLs. (f) θ:2θ XRD patterns of compact $CsPb(I_{1-x}Br_x)_3$ NC SL films. Corresponding x-values are indicated next to each pattern. The dashed vertical gray line at ~30° 2θ indicates the approximate peak position for $x = 1.00$ NC SLs. Patterns offset for clarity. (g) Zoomed-in view of the ~15° 2θ (Cu Kα) peaks in panel f, which are replotted on a logarithmic intensity scale versus scattering vector ($Q = [4\pi/\lambda_{Cu}]\sin[\theta]$). Asterisks in $x = 0$ patterns in panels f and g indicate peaks related to 0D Cs_4PbI_6 NCs.

(Figure 1a) and emission (Figure 1b) following illumination (before, dashed red lines; after, solid blue lines). Figure 1b shows that the PL peak energy blueshifts ≈320 meV from $E_{PL,Max} \approx 2.07$ eV to $E_{PL,Max} \approx 2.39$ eV. These spectral changes are qualitatively consistent with a compositional transformation from $CsPb(I_{1-x}Br_x)$ with $x = 0.36$ into pure $CsPbBr_3$ NCs.

The overall appearance of the absorption spectrum following illumination (Figure 1a, solid blue line) closely resembles that observed in the initial spectrum prior to illumination (Figure 1a, dashed red line). The major difference is a large blueshift. This suggests that the NCs have not been destroyed. Transmission electron microscopy (TEM) images before and after illumination (Figure 1c,d) verify that the NCs preserve their cuboidal morphology. Curiously, the average edge lengths after illumination ($l = 7.1 \pm 0.6$ nm) are near identical to that before illumination ($l = 7.1 \pm 0.7$ nm). Figure 1, therefore, points to dynamic photochemistry occurring within mixed halide NCs under irradiation that is clearly different from the corresponding response of counterpart polycrystalline thin films.[20−24] To understand how illuminating mixed halide NCs alters their optical response yet apparently preserves their structure, we survey the photostability of shape- and size-pure, mixed halide perovskite NC SLs.

Mixed Halide $CsPb(I_{1-x}Br_x)_3$ NC SLs. In total, eight distinct $CsPb(I_{1-x}Br_x)_3$ ($0 < x < 1.00$) perovskite NC SL compositions were fabricated. The $CsPb(I_{1-x}Br_x)_3$ NC ensembles, employed in self-assembly, were synthesized using modified literature procedures.[1,15−17] TEM images in Figure S3 show that all eight NC ensembles adopt cuboidal morphologies with average edge

https://dx.doi.org/10.1021/acsenergylett.0c00630
ACS Energy Lett. 2020, 5, 1465−1473

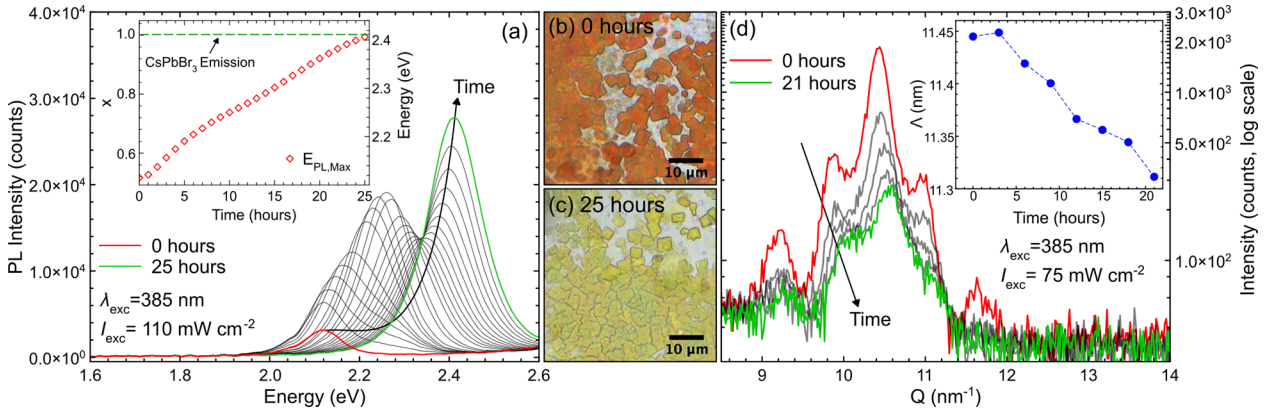

Figure 3. (a) Time-evolved emission spectra in 1 h segments (gray lines) for an x = 0.47 NC SL film over 25 h of CW illumination (λ_{exc} = 385 nm, I_{exc} = 110 mW cm^{-2}). Inset: $E_{PL,Max}$ and x versus time. The dashed green line represents the emission energy of a single $CsPbBr_3$ NC SL (x = 1.00). Optical microscopy images of x = 0.47 NC SLs (b) before and (c) after 25 h of illumination. (d) In situ θ:2θ XRD patterns of a x = 0.47 NC SL film over 21 h of CW illumination (λ_{exc} = 385 nm, I_{exc} = 75 mW cm^{-2}). Inset: Λ-values over time under illumination.

lengths in the range of l = 8.5−11.6 nm and size-distributions of ∼10% (see Table S1). NC SLs were grown from concentrated NC dispersions in toluene or tetrachloroethylene on top of 1 × 1 cm Si substrates by slow solvent evaporation.[28,29] Details of NC synthesis and composition tuning (Figure S4), self-assembly, size characterization by TEM, and halide composition quantification via scanning electron microscopy-energy dispersive X-ray spectroscopy (SEM-EDS) can be found in the Supporting Information.

Figure 2a shows a high-angle annular dark-field scanning TEM (HAADF-STEM) image of a $CsPb(I_{0.50}Br_{0.50})_3$ NC SL, where individual NCs are apparent. The inset of Figure 2a is a zoomed out HAADF-STEM image of an entire mixed halide NC SL. Figure 2b−e illustrates representative optical microscopy images of $CsPb(I_{1-x}Br_x)_3$ NC SLs ($0 < x < 1.00$). The insets in Figure 2b−d are true color, spatially resolved PL maps obtained from confocal laser scanning microscopy (CLSM). The colors of SL PL shift from red to green as x decreases with a corresponding PL energy ranging from ∼1.8 eV (x = 0) to ∼2.4 eV (x = 1.00). Figure S5 shows ensemble NC absorption/PL in toluene as well as single SL PL spectra and optical microscopy images for each x-value. Figure S6 illustrates individual NC SL emission maps for all halide compositions. Figure S7 shows the halide composition calibration curves based on absorption/PL energies. Details of these optical measurements are provided in the Supporting Information.

θ:2θ XRD measurements of compact $CsPb(I_{1-x}Br_x)_3$ NC SL films (Figure 2f) demonstrate the strong preferred orientation of NCs normal to SL surfaces in the pseudocubic ⟨100⟩ direction.[2,38−42] Peaks at ∼15° 2θ and ∼30° 2θ stem from the pseudocubic (100) and (200) planes, respectively. Evident in Figure 2f is a shift of both (100) and (200) reflections from lower to higher degrees 2θ with increasing x.[1,15,16] XRD patterns for all halide compositions are summarized in Figure S8 along with details of the XRD measurements. Table S1 lists the approximate angles of (200) atomic Bragg reflections, and Figure S9 provides an associated XRD-based compositional calibration curve. The extra peak at ∼12.1° 2θ x = 0 (top, dark red lines denoted with an asterisk in Figure 2f,g) arises from the occurrence of a Cs_4PbI_6 impurity.[43]

Beyond strongly preferred NC orientation, perovskite NC SL structural coherence is evident through SL reflections.[29] SL reflections are most recognizable by the fine structure of reflections at 2θ ≈ 15°.[29] These SL reflections emerge, according to Bragg's law, at $Q_n = 2\pi n/\Lambda$ (derived by substituting Q for sin θ),[29] with Q_n the scattering vector associated with the nth order satellite peak maximum intensity, n an integer representing the SL reflection diffraction order, and Λ the NC-to-NC (core-to-core) interparticle spacing (i.e., the SL periodicity).

Figure 2g better illustrates the (100) SL satellite peak splitting, showing zoomed-in logarithmic intensity scale versus scattering vector (Q) diffraction patterns. Two to five SL reflections are identifiable for each composition, with Table S1 summarizing fit-extracted Λ for all compositions. Such SL reflections have been unintentionally[14,18,44−47] observed in prior XRD studies.

Light-Induced Optical and Structural Changes in $CsPb(I_{1-x}Br_x)_3$ NC SLs. Figure 3a illustrates the PL spectra of an x = 0.47 NC SL film collected over 25 h (spectra shown in 1 h increments) under CW illumination (λ_{exc} = 385 nm; I_{exc} = 110 mW cm^{-2}). Similar to NCs in solution (Figures 1a,b), spectral blueshifts occur in the NC SLs. The inset of Figure 3a plots this gradual blueshift from $E_{PL,Max}$ = 2.115 to 2.406 eV (586 to 515 nm); the latter value is consistent with that of pure $CsPbBr_3$ NC SLs (indicated by the horizontal, dashed green line). Figure S10 shows similar PL spectral shifting for an x = 0.72 NC SL film. These spectral changes are irreversible when returned to the dark for 21 h (Figure S11). Furthermore, photoinduced blueshifts are unique to mixed halide NC SLs and do not occur with single halide materials. This has been demonstrated through control tests conducted under identical illumination conditions on single-halide $CsPbI_3$ and $CsPbBr_3$ NC SLs. Both $CsPbI_3$ and $CsPbBr_3$ NC SLs experience emission intensity decreases without significant shifts in their $E_{PL,Max}$ (Figure S12). As a note, the CW illumination intensities (I_{exc} ≈ 75−110 mW·cm^{-2}) used in this work are comparable to average intensities (I_{exc} ≈ 5−200 mW·cm^2) employed with pulsed lasers (λ_{exc} = 400 nm, 1 kHz repetition rate) in prior optical amplification experiments on lead halide perovskite NC films.[48−50] Amplified spontaneous emission and other phenomena requiring intense irradiation of mixed halide NC films will likely be complicated by the light-induced changes observed in the NC SL films (Figure 3).

Next, optical microscopy images (Figures 3b,c) indicate that the cuboidal morphologies of mixed halide NC SLs are preserved during CW illumination, despite evident color

https://dx.doi.org/10.1021/acsenergylett.0c00630
ACS Energy Lett. 2020, 5, 1465−1473

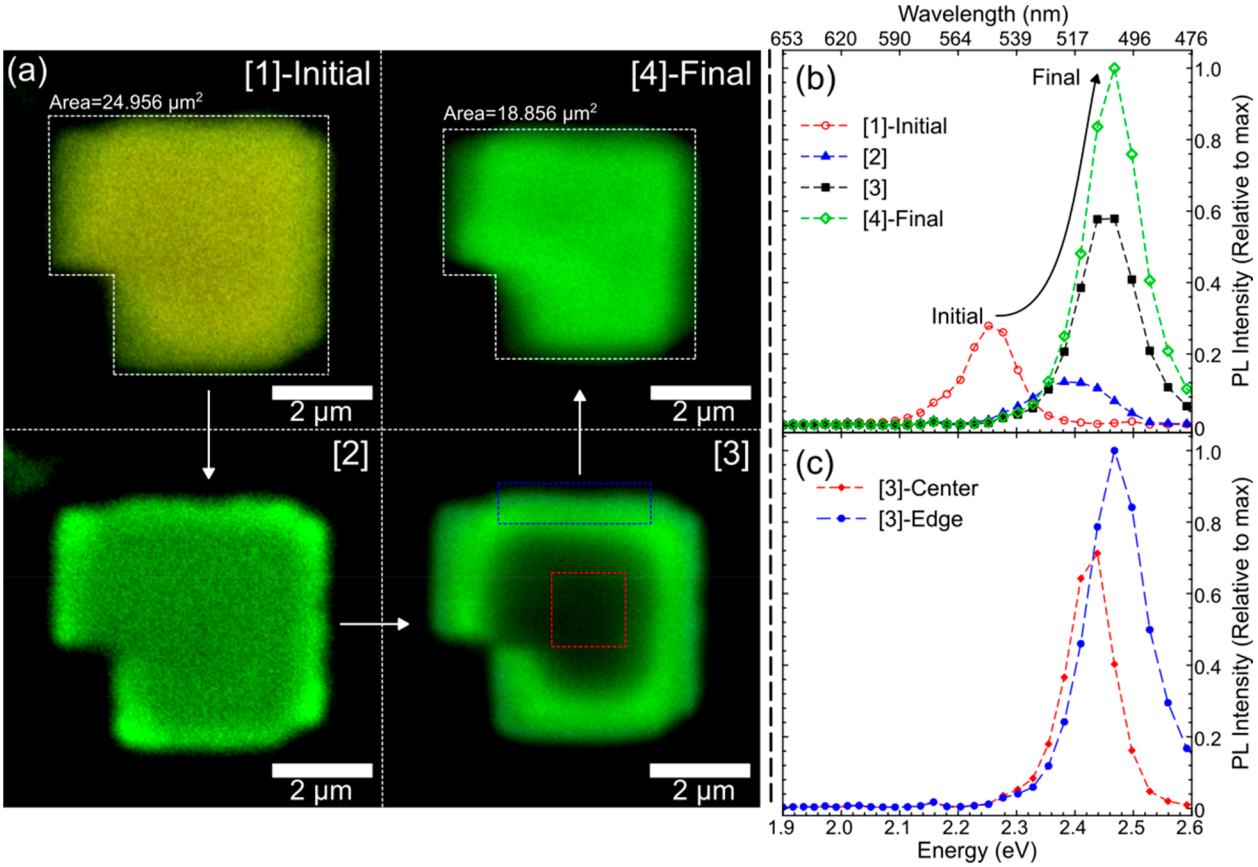

Figure 4. Spatially resolved PL maps (7.50 × 7.50 μm) of an individual x = 0.72 $CsPb(I_{0.28}Br_{0.72})_3$ NC SL after three rounds ([1], initial; [2], one round; [3], two rounds; and [4], three rounds) of brief, intense CW laser illumination in a scanning confocal microscope (λ_{exc} = 405 nm; nominal $I_{exc} \approx 1.7 \times 10^7$ W cm^{-2}; exposure time per round, ~120 μs). Dashed white lines and numbers in [1] and [2] represent the approximate area of the NC SL. (b) Averaged PL spectra from all pixels within the NC SL from the four images in panel a. (c) PL spectra from the center (edge) of the SL, as indicated using a dashed red line (dashed blue line) in PL map [3] of panel a.

changes from red-orange (mixed halide, Figure 3b) to yellow ($CsPbBr_3$, Figure 3c). In addition, optical microscopy measurements show no gross changes to the physical dimensions of the irradiated NC SLs. This SL behavior resembles that seen in Figure 1c,d for individual NCs illuminated in solution. SEM-EDS measurements of NC SLs before and after illumination verify increases in x-values (from x = 0.47 to x = 0.63) and point to partial I^- expulsion from component NCs.

To further explore light-induced structural changes in NC SLs, Figure 3d plots time-elapsed XRD patterns of SL (100) Bragg reflections from a compact x = 0.47 SL film over 21 h of CW illumination (λ_{exc} = 385 nm, I_{exc} = 75 mW cm^{-2}). The center of the reflections progressively shifts to higher scattering vectors over time, indicating a contraction of the perovskite structure. In particular, SL (200) reflections shift from $Q_n \approx$ 20.856 nm^{-1} to $Q_n \approx$ 21.198 nm^{-1} and correspond to a decrease of the pseudocubic structure parameter from 6.025 to5.927 Å. The final scattering vector and structure parameters are near those of pure $CsPbBr_3$ NC SLs ($Q_n \approx$ 21.338 nm^{-1}; 5.840 Å[51]), corroborating the conclusions derived from the above-mentioned PL measurements.

These light-induced changes to NC SL XRD patterns are irreversible (checked after 21 h in the dark, Figure S13) and, in whole, point to a near-complete and light-induced structure-preserving transformation of NC SLs from $CsPbBr(I_{1-x}Br_x)_3$ to $CsPbBr_3$. This is indirectly seen through the preservation of NC SL shapes in Figure 3b,c. It is remarkable then, that despite the significant compositional changes, NCs within SLs retain their close-packed structural order during and after observed photoinduced changes. This is directly observed by retaining SL reflections over time (Figure 3d), which indicates that despite the photoinduced changes, the NCs remain size- and shape-pure under illumination. Simultaneously, fit-extracted Λ-values in Figure 3d (inset) decrease slightly from ~11.44 nm to ~11.31 nm and verify that NC l-values do not significantly change under illumination. This agrees with the data in Figure 1c,d.

We now survey individual NC SLs via CLSM to provide deeper insight into the relationship between light-induced structural changes and the optical response of mixed halide NCs. Figure 4a shows spatially resolved, true color PL maps of an individual x = 0.72 NC SL before and after three rounds ([1], initial; [2], after one round; [3], after two rounds; and [4], after three rounds) of brief, intense CW laser irradiation in a CLSM (λ_{exc} = 405 nm; $I_{exc} \approx 1.7 \times 10^7$ W cm^{-2}; exposure time per round ~120 μs, see the Supporting Information for more details). Evident is a change in the emission color from yellow (Figure 4a, [1]) to green (Figure 4a, [4]). Also apparent is that the color change starts from the outside of the SL and progressively moves toward its inside (i.e., Figure 4a, [2] and [3]). These spectral changes are summarized in Figure 4b, which plots PL spectra for each map in Figure 4a (averaged from all pixels within SLs). The data shows that in addition to

https://dx.doi.org/10.1021/acsenergylett.0c00630
ACS Energy Lett. 2020, 5, 1465−1473

a PL peak blueshift from ≈2.25 to ≈2.47 eV (551 to 503 nm), there is an apparent photobrightening effect. Figure 4c compares PL spectra from the SL edge (dashed blue line/circles) to its center (dashed red line/diamonds) using the PL map in Figure 4a, [3]. This data shows that the edge-emission is brighter and higher in energy than the corresponding emission from the center. The PL maps in Figure 4a were chosen at representative intermediate points during NC SL photoinduced conversion. The Supporting Information shows a CLSM movie (Movie S1) of this entire energy shift and photobrightening.

The movie and images show that beyond spectral changes, which remain to be explained, the NC SLs maintain their general morphology during irradiation. They do shrink by a few hundred nanometers in each observable dimension (areas indicated by dashed white lines in Figure 4a, [1] and [4]), where for the particular SL studied, the overall area decreases from ∼25 to 19 μm^2 (a ∼24% drop). This decrease is *not* consistent with the structural contractions seen in Figure 3d because a ∼1.1% change of component NCs (i.e., Λ decreases from 11.44 to 11.31 nm) translates only to an expected ∼2.3% change of the visible SL surface area. This discrepancy and the dynamic spectral changes in Figure 4 hint at an unusual photochemical transformation of the SL.

Origin of Photoinduced NC and SL Transformations. We now speculate that PL blueshifts and SL structural contractions stem from irreversible I_2 sublimation from component NCs during illumination.[27] This is motivated by earlier works on bulk lead halide photooxidation chemistries, which show irradiation-induced I_2 sublimation.[52,53] More recent work by Zhang et al.[27] also suggests that I_2 sublimation may occur in mixed halide perovskite NCs under illumination. We have therefore checked this hypothesis using a simple indicator test. Briefly, a strip of paper carrying a small amount of dried potassium iodide (KI) and potato starch mixture is enclosed in a vial with dried, mixed halide NC SLs (x = 0.50). NCs in the vial are then illuminated for 20 h (λ_{exc} = 470 nm, I_{exc} = 80 mW cm^{-2}). Following the illumination, the original white test strip exhibited yellow stains characteristic of the I_3^-/starch complex. The complex results from the reaction of I_2 with KI-derived I^- (see the discussion in the Supporting Information and Figures S14 and S15 for more details).

The following mechanism is then proposed to explain the photoinduced changes reported in Figures 3 and 4. Under illumination, the photogenerated holes reduce I^- to I^0 within component NCs of the SL.[52−56] Because of the larger excitation intensity present at SL surfaces, their outermost NCs experience I^- reduction first. Once a suitable density of I^0 is generated, I_2 forms, leaving both component NCs and parent SLs as I_2 gas.

Continued irradiation eventually destroys the outermost NC layer(s), leaving a SL surface enriched in Br^- anions surrounded by oleylammonium, Cs^+, or Pb^{2+} counterions. The outermost NC layers in SLs therefore act as sacrificial layers to generate an excess of bromide species. In tandem, the NCs further inside the SL experience I^- reduction and I_2 evolution. However, SL surfaces now contain an excess of Br^- ions, which can diffuse through the SL to fill internal iodine vacancies.[15,16] Continued irradiation promotes this process and ultimately converts the component mixed halide NCs of the parent SL into $CsPbBr_3$ NCs. The process is self-limited by the amount of I^- present in the original mixed halide material.

At the same time, Pb^{2+} and Cs^+, remaining from the degraded NCs at the surface of the SLs, interact with atmospheric oxygen, water, and remaining organic ligands to chemically passivate NC and SL surfaces. This amorphous surface layer along with excess Br^- may then be responsible for the observed PL photobrightening that occurs by virtue of passivating surface-related trap states of individual NCs.[57−61] In total, the proposed mechanism qualitatively rationalizes the observations made in Figures 3 and 4. Specifically, SL emission blueshifts despite little change to the component NC dimensions with spectral changes commencing at the edges then moving inward, leading to SL contraction.

To further investigate the mechanism as well as the existence of photodegraded NC surface layers on irradiated SLs, TEM images and selected area electron diffraction (SAED) patterns were acquired on individual $CsPb(I_{0.50}Br_{0.50})_3$ NC SLs before (Figures 5a,b) and after (Figures 5c,b) 24 h of CW laser

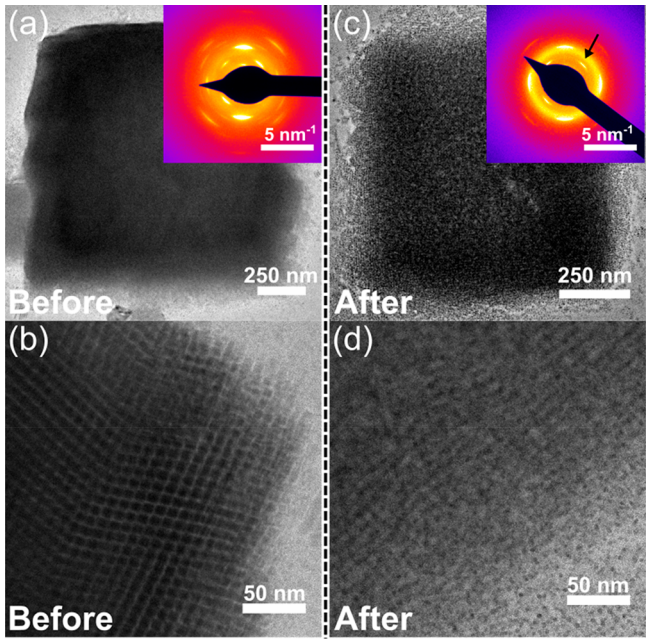

Figure 5. TEM image of $CsPb(I_{0.50}Br_{0.50})_3$ NC SLs from the same TEM grid before (a and b) and after (c and d) 24 h of CW illumination (λ_{exc} = 405 nm; I_{exc} = 100 mW cm^{-2}). Insets of panels a and c are selected area electron diffraction patterns of the associated NC SLs.

illumination (λ_{exc} = 405 nm; I_{exc} = 100 mW cm^{-2}). TEM-EDS maps in Figure S16 confirm significant I^- losses after illumination while SAED patterns before/after illumination (insets in Figures 5a,c) demonstrate that NCs within SLs retain their perovskite crystal structure. This is consistent with the XRD experiments discussed above (Figure 3d). However, the outlines of individual NCs are much harder to resolve following the illumination (compare panels b and d of Figure 5). Moreover, postilluminated SAED patterns contain a broad ring (Figure 5c, inset, indicated by the black arrow) absent in starting samples. These latter observations suggest that the NC SLs are covered by an amorphous layer, resulting from CW laser illumination. The existence of an amorphous coating is also observed in associated SEM images (Figures S17).

To further quantify the anion stoichiometry of irradiated SLs and address the makeup of their amorphous surface layer, X-ray photoemission spectroscopy (XPS) on pristine and

https://dx.doi.org/10.1021/acsenergylett.0c00630
ACS Energy Lett. 2020, 5, 1465−1473

illuminated replicas of x = 0.36 NC SL films was performed (Figure S18). These XPS results reveal that the atomic percentage of iodine in SLs decreases from 42.1% to 15.8% during illumination. This is consistent with the aforementioned SEM-EDS and TEM-EDS analyses. Moreover, an increase in the atomic % of Pb^{2+} (20.3% to 42.0%) is observed after illumination, suggesting that the topmost layer of the sample is enriched in Pb. The surface layer is therefore likely an amorphous mixture containing Pb−I and Pb−O species, formed as a result of photochemical reactions with oxygen and water from the air.[57−61]

To conclude, $CsPb(I_{1-x}Br_x)_3$ NC SLs with a high degree of compositional tunability that can be harnessed to precisely engineer their collective optical and electronic response have been demonstrated. Under prolonged optical illumination, the NC and SL morphologies, size, and structural coherence are maintained. That is remarkable, given the near-complete expulsion of almost half of the anions from the perovskite crystal structure under CW illumination. In a broader context, such stability demonstrates the robustness of the cation substructure of lead halide perovskites and the ligand shell of NCs, which template both NC size and SL shape. At the same time, our results highlight the clear need not only to better understand the driving forces behind these photoinduced changes but also to stabilize mixed halide NC SLs against undesired photochemistry. In the former, I_{exc}-dependent measurements (similar to prior reports for mixed halide thin film counterparts)[20−22] would reveal critical information about the underlying I_2 sublimation kinetics.[52] In the latter, encapsulating particles with inorganic shells (e.g., $PbSO_4$) represents a viable method to improve the photostability of mixed halide perovskite NCs.[62]

■ ASSOCIATED CONTENT

Supporting Information

The Supporting Information is available free of charge at https://pubs.acs.org/doi/10.1021/acsenergylett.0c00630.

Materials and methods, PL spectra of $CsPb(I_{0.64}Br_{0.36})_3$ NCs in toluene during 25 min of CW illumination and absorption and PL spectra of the sample after it was stored in the dark for 17 h; representative TEM images of all mixed halide NCs used in the SL growth; tabulated SEM-EDS, TEM, absorption, PL, and XRD data for $CsPb(I_{1-x}Br_x)_3$ NCs in solution and SLs; absorption and PL spectra of NCs in toluene as well as single SL emission spectra; optical microscopy images of SLs for all halide compositions; individual NC SL CLSM PL maps for all halide compositions; halide composition calibration curves based on absorption and PL energies; XRD patterns for the NC SLs of all halide compositions; XRD-based halide composition calibration curve; time evolution of PL spectra for an x = 0.72 NC SL film under illumination; PL recovery spectra of NC SL films (x = 0.47, 0.72) kept in the dark for 21 h; control experiments showing time evolution of PL spectra of single-halide $CsPbI_3$ and $CsPbBr_3$ NC SLs under illumination; results of the potato starch/potassium iodide indicator test; TEM-EDS maps and SEM images of NC SLs before and after illumination; XPS spectra of as-made and illuminated replicas of x = 0.36 NC SL films (PDF)

Movie of the spatially inhomogeneous emission blueshift and photobrightening for an x = 0.72 NC SL shown in Figure 4 (MOV)

■ AUTHOR INFORMATION

Corresponding Authors

Michael C. Brennan − *Department of Chemistry and Biochemistry, University of Notre Dame, Notre Dame, Indiana 46556, United States; International Doctoral Program in Science, Università Cattolica del Sacro Cuore, 25121 Brescia, Italy;* orcid.org/0000-0002-4482-5173; Email: mbrenn13@nd.edu

Masaru Kuno − *Department of Chemistry and Biochemistry and Department of Physics, University of Notre Dame, Notre Dame, Indiana 46556, United States;* orcid.org/0000-0003-4210-8514; Email: mkuno@nd.edu

Liberato Manna − *Nanochemistry Department, Istituto Italiano di Tecnologia, 16163 Genova, Italy;* orcid.org/0000-0003-4386-7985; Email: liberato.manna@iit.it

Dmitry Baranov − *Nanochemistry Department, Istituto Italiano di Tecnologia, 16163 Genova, Italy;* orcid.org/0000-0001-6439-8132; Email: dmitry.baranov@iit.it

Authors

Stefano Toso − *International Doctoral Program in Science, Università Cattolica del Sacro Cuore, 25121 Brescia, Italy; Nanochemistry Department, Istituto Italiano di Tecnologia, 16163 Genova, Italy*

Ilia M. Pavlovetc − *Department of Chemistry and Biochemistry, University of Notre Dame, Notre Dame, Indiana 46556, United States*

Maksym Zhukovskyi − *Notre Dame Integrated Imaging Facility, University of Notre Dame, Notre Dame, Indiana 46556, United States*

Sergio Marras − *Materials Characterization Facility, Istituto Italiano di Tecnologia, 16163 Genova, Italy*

Complete contact information is available at: https://pubs.acs.org/10.1021/acsenergylett.0c00630

Notes

The authors declare no competing financial interest.

■ ACKNOWLEDGMENTS

M.C.B. acknowledges support from Patrick and Jana Eilers Graduate Student Fellowship and the Notre Dame Radiation Laboratory (NDRL) for use of its facilities. The NDRL is supported by the U.S. Department of Energy Office of Science, Office of Basic Energy Sciences under Award Number DE-FC02- 04ER15533. This is contribution number NDRL No. 5275. M.Z. thanks the University of Notre Dame Integrated Imaging Facility for financial support of the work conducted on this project. M.K. and M.C.B. acknowledge support the from the Division of Materials Sciences and Engineering, Office of Basic Energy Sciences, U.S. Department of Energy under award DE-SC0014334. D.B. was supported by the European Union's Horizon 2020 research and innovation programme under the Marie Sklodowska-Curie Grant Agreement No. 794560 (RETAIN). D.B. and M.C.B. thank Dr. Mirko Prato for performing XPS measurements and Dr. Marco Salerno (both Materials Characterization Facility at IIT) for training and technical support with the operation of ZETA-20 true color 3D optical profiler used for NC SLs optical imaging.

https://dx.doi.org/10.1021/acsenergylett.0c00630
ACS Energy Lett. 2020, 5, 1465−1473

REFERENCES

(1) Protesescu, L.; Yakunin, S.; Bodnarchuk, M. I.; Krieg, F.; Caputo, R.; Hendon, C. H.; Yang, R. X.; Walsh, A.; Kovalenko, M. V. Nanocrystals of Cesium Lead Halide Perovskites ($CsPbX_3$, X= Cl, Br, and I): Novel Optoelectronic Materials Showing Bright Emission with Wide Color Gamut. *Nano Lett.* **2015**, *15*, 3692−3696.

(2) Swarnkar, A.; Marshall, A. R.; Sanehira, E. M.; Chernomordik, B. D.; Moore, D. T.; Christians, J. A.; Chakrabarti, T.; Luther, J. M. Quantum Dot-Induced Phase Stabilization of α-$CsPbI_3$ Perovskite for High-Efficiency Photovoltaics. *Science* **2016**, *354*, 92−95.

(3) Sanehira, E. M.; Marshall, A. R.; Christians, J. A.; Harvey, S. P.; Ciesielski, P. N.; Wheeler, L. M.; Schulz, P.; Lin, L. Y.; Beard, M. C.; Luther, J. M. Enhanced Mobility $CsPbI_3$ Quantum Dot Arrays for Record-Efficiency, High Voltage Photovoltaic Cells. *Sci. Adv.* **2017**, *3*, 4204.

(4) Kovalenko, M. V.; Protesescu, L.; Bodnarchuk, M. I. Properties and Potential Optoelectronic Applications of Lead Halide Perovskite Nanocrystals. *Science* **2017**, *358*, 745−750.

(5) Akkerman, Q. A.; Raino, G.; Kovalenko, M. V.; Manna, L. Genesis, Challenges and Opportunities for colloidal lead Halide Perovskite Nanocrystals. *Nat. Mater.* **2018**, *17*, 394−405.

(6) Huang, H.; Bodnarchuk, M. I.; Kershaw, S. V.; Kovalenko, M. V.; Rogach, A. L. Lead Halide Perovskites Nanocrystals in the Research Spotlight: Stability and Defect Tolerance. *ACS Energy Lett.* **2017**, *2*, 2071−2083.

(7) Morozov, Y. V.; Zhang, S.; Brennan, M. C.; Janko, B.; Kuno, M. Photoluminescence Up-Conversion in $CsPbBr_3$ Nanocrystals. *ACS Energy Lett.* **2017**, *2*, 2514−2515.

(8) Zhang, S.; Zhukovskyi, M.; Janko, B.; Kuno, M. Progress in Laser Cooling Semiconductor Nanocrystals and Nanostructures. *NPG Asia Mater.* **2019**, *11*, 54.

(9) Liu, F.; Zhang, Y.; Ding, C.; Kobayashi, S.; Izuishi, T.; Nakazawa, N.; Toyoda, T.; Ohta, T.; Hayase, S.; Minemoto, T.; Yoshino, K.; Dai, S.; Shen, Q. Highly Luminescent Phase-Stable $CsPbI_3$ Perovskite Quantum Dots Achieving Near 100% Absolute Photoluminescence Quantum Yield. *ACS Nano* **2017**, *11*, 10373−10383.

(10) Pan, J.; Shang, Y.; Yin, J.; De Bastiani, M.; Peng, W.; Dursun, I.; Sinatra, L.; El-Zohry, A.; Hedhili, M. N.; Emwas, A. H.; Mohammed, O. F.; Ning, Z.; Bakr, O. M. Bidentate Ligand-Passivated $CsPbI_3$ Perovskite Nanocrystals for Stable Near-Unity Photoluminescence Quantum Yield and Efficient Red Light-Emitting Diodes. *J. Am. Chem. Soc.* **2018**, *140*, 562−565.

(11) Di Stasio, F.; Christodoulou, S.; Huo, N.; Konstantatos, G. Near-Unity Photoluminescence Quantum Yield in $CsPbBr_3$ Nanocrystal Solid-State Films via Postsynthesis Treatment with Lead Bromide. *Chem. Mater.* **2017**, *29*, 7663−7667.

(12) Koscher, B. A.; Swabeck, J. K.; Bronstein, N. D.; Alivisatos, P. A. Essentially Trap-Free $CsPbBr_3$ Colloidal Nanocrystals by Postsynthetic Thiocyanate Surface Treatment. *J. Am. Chem. Soc.* **2017**, *139*, 6566−6569.

(13) Brennan, M. C.; Zinna, J.; Kuno, M. Existence of a Size-Dependent Stokes Shift in $CsPbBr_3$ Perovskite Nanocrystals. *ACS Energy Lett.* **2017**, *2*, 1487−1488.

(14) Brennan, M. C.; Herr, J. E.; Nguyen-Beck, T. S.; Zinna, J.; Draguta, S.; Rouvimov, S.; Parkhill, J.; Kuno, M. Origin of the Size-Dependent Stokes Shift in $CsPbBr_3$ Perovskite Nanocrystals. *J. Am. Chem. Soc.* **2017**, *139*, 12201−12208.

(15) Nedelcu, G.; Protesescu, L.; Yakunin, S.; Bodnarchuk, M. I.; Grotevent, M. J.; Kovalenko, M. V. Fast Anion-Exchange in Highly Luminescent Nanocrystals of Cesium Lead Halide Perovskite ($CsPbX_3$, X = Cl, Br, I). *Nano Lett.* **2015**, *15*, 5635−5640.

(16) Akkerman, Q. A.; D'Innocenzo, V.; Accornero, S.; Scarpellini, A.; Petrozza, A.; Prato, M.; Manna, L. Tuning the Optical Properties of Cesium Lead Halide Perovskite Nanocrystals by Anion Exchange Reactions. *J. Am. Chem. Soc.* **2015**, *137*, 10276−10281.

(17) Almeida, G.; Goldoni, L.; Akkerman, Q.; Dang, Z.; Khan, A. H.; Marras, S.; Moreels, I.; Manna, L. Role of Acid-Base Equilibria in the Size, Shape, and Phase Control of Cesium Lead Bromide Nanocrystals. *ACS Nano* **2018**, *12*, 1704−1711.

(18) Imran, M.; Ijaz, P.; Baranov, D.; Goldoni, L.; Petralanda, U.; Akkerman, Q.; Abdelhady, A. L.; Prato, M.; Bianchini, P.; Infante, I.; Manna, L. Shape-Pure, Nearly Monodispersed $CsPbBr_3$ Nanocubes Prepared Using Secondary Aliphatic Amines. *Nano Lett.* **2018**, *18*, 7822−7831.

(19) Dong, Y.; Qiao, T.; Kim, D.; Parobek, D.; Rossi, D.; Son, D. H. Precise Control of Quantum Confinement in Cesium Lead Halide Perovskite Quantum Dots via Thermodynamic Equilibrium. *Nano Lett.* **2018**, *18*, 3716−3722.

(20) Brennan, M. C.; Draguta, S.; Kamat, P. V.; Kuno, M. Light-Induced Anion Phase Segregation in Mixed Halide Perovskites. *ACS Energy Lett.* **2018**, *3*, 204−213.

(21) Brennan, M. C.; Ruth, A.; Kamat, P.; Kuno, M. Photoinduced Anion Segregation in Mixed Halide Perovskites. *Trends in Chemistry* **2020**, *2*, 282−301.

(22) Draguta, S.; Sharia, O.; Yoon, S. J.; Brennan, M. C.; Morozov, Y. V.; Manser, J.; Kamat, P. V.; Schneider, W. F.; Kuno, M. Rationalizing the Light-Induced Phase Separation of Mixed Halide Organic-Inorganic Perovskites. *Nat. Commun.* **2017**, *8*, 200.

(23) Ruth, A.; Brennan, M. C.; Draguta, S.; Morozov, Y. V.; Zhukovskyi, M.; Janko, B.; Zapol, P.; Kuno, M. Vacancy-Mediated Anion Photosegregation Kinetics in Mixed Halide Hybrid Perovskites: Coupled Kinetic Monte Carlo and Optical Measurements. *ACS Energy Lett.* **2018**, *3*, 2321.

(24) Hoke, E. T.; Slotcavage, D. J.; Dohner, E. R.; Bowring, A. R.; Karunadasa, H. I.; McGehee, M. D. Reversible Photo-Induced Trap Formation in Mixed-Halide Hybrid Perovskites for Photovoltaics. *Chem. Sci.* **2015**, *6*, 613−617.

(25) Gualdrón-Reyes, A. F.; et al. Controlling the Phase Segregation in Mixed Halide Perovskites through Nanocrystal Size. *ACS Energy Lett.* **2019**, *4*, 54−62.

(26) Wang, Xi.; Ling, Y.; Lian, X.; Xin, Y.; Dhungana, K. B.; Perez-Orive, F.; Knox, J.; Chen, Z.; Zhou, Y.; Beery, D.; Hanson, K.; Shi, J.; Lin, S.; Gao, H. Suppressed Phase Separation of Mixed-Halide Perovskites Confined in Endotaxial Matrices. *Nat. Commun.* **2019**, *10*, 695.

(27) Zhang, H.; Fu, X.; Tang, Y.; Wang, H.; Zhang, C.; Yu, W. W.; Wang, X.; Zhang, Y.; Xiao, M. Phase Segregation due to Ion Migration in All-Inorganic Mixed-Halide Perovskite Nanocrystals. *Nat. Commun.* **2019**, *10*, 1088.

(28) Baranov, D.; Toso, S.; Imran, M.; Manna, L. Investigation into the Photoluminescence Red Shift in Cesium Lead Bromide Nanocrystal Superlattices. *J. Phys. Chem. Lett.* **2019**, *10*, 655−660.

(29) Toso, S.; Baranov, B.; Giannini, C.; Marras, S.; Manna, L. Wide-Angle X-Ray Diffraction Evidence of Structural Coherence in $CsPbBr_3$ Nanocrystal Superlattices. *ACS Materials Lett.* **2019**, *1*, 272−276.

(30) Jurow, M. J.; Lampe, T.; Penzo, E.; Kang, J.; Koc, M. A.; Zechel, T.; Nett, Z.; Brady, M.; Wang, L.-W.; Alivisatos, A. P.; et al. Tunable Anisotropic Photon Emission from Self-Organized $CsPbBr_3$ Perovskite Nanocrystals. *Nano Lett.* **2017**, *17*, 4534−4540.

(31) Rainò, G.; Becker, M. A.; Bodnarchuk, M. I.; Mahrt, R. F.; Kovalenko, M. V.; Stöferle, T. Superfluorescence from Lead Halide Perovskite Quantum Dot Superlattices. *Nature* **2020**, *563*, 671.

(32) Nagaoka, Y.; Hills-Kimball, K.; Tan, R.; Li, R.; Wang, Z.; Chen, O. Nanocube Superlattices of Cesium Lead Bromide Perovskites and Pressure-Induced Phase Transformations at Atomic and Mesoscale Levels. *Adv. Mater.* **2017**, *29*, 1606666.

(33) Tong, Y.; Yao, E.-P.; Manzi, A.; Bladt, E.; Wang, K.; Döblinger, M.; Bals, S.; Müller-Buschbaum, P.; Urban, A. S.; Polavarapu, L.; et al. Spontaneous Self-Assembly of Perovskite Nanocrystals into Electronically Coupled Supercrystals: Towards Filling the Green Gap. *Adv. Mater.* **2018**, *30*, 1801117.

(34) Kovalenko, M. V.; Bodnarchuk, M. I. Lead Halide Perovskite Nanocrystals: From Discovery to Self-Assembly and Applications. *Chimia* **2017**, *71*, 461−470.

(35) Thomas, C. J.; Zhang, Y.; Guillaussier, A.; Bdeir, K.; Aly, O. F.; Kim, H. G.; Noh, J.; Reimnitz, L. C.; Li, J.; Deepak, F. L.; Smilgies,

https://dx.doi.org/10.1021/acsenergylett.0c00630
ACS Energy Lett. 2020, 5, 1465−1473

D.-M.; Milliron, D. J.; Korgel, B. A. *Chem. Mater.* **2019**, *31*, 9750−9758.
(36) Jagielski, J.; Solari, F. S.; Jordan, L.; Scullion, D.; Blulle, B.; Li, Y.-T.; Krumeich, F.; Chiu, Y.-C.; Ruhstaller, B.; Santos, E. J. G.; Shih, C.-J. Scalable Photonic Sources using Two-Dimensional Lead Halide Perovskite Superlattices. *Nat. Commun.* **2020**, *11*, 387.
(37) Zhou, C.; Zhong, Y.; Dong, H.; Zheng, W.; Tan, J.; Jie, Q.; Pan, A.; Zhang, L.; Xie, W. Cooperative Excitonic Quantum Ensemble in Perovskite-Assembly Superlattice Microcavities. *Nat. Commun.* **2020**, *11*, 329.
(38) Cottingham, P.; Brutchey, R. L. On the Crystal Structure of Colloidally Prepared $CsPbBr_3$ Quantum Dots. *Chem. Commun.* **2016**, *52*, 5246−5249.
(39) Cottingham, P.; Brutchey, R. L. Depressed Phase Transitions and Thermally Persistent Local Distortions in $CsPbBr_3$ Quantum Dots. *Chem. Mater.* **2018**, *30*, 6711−6716.
(40) Bertolotti, F.; Protesescu, L.; Kovalenko, M. V.; Yakunin, S.; Cervellino, A.; Billinge, S. J.; Terban, M. W.; Pedersen, J. S.; Masciocchi, N.; Guagliardi, A. Coherent Nanotwins and Dynamic Disorder in Cesium Lead Halide Perovskite Nanocrystals. *ACS Nano* **2017**, *11*, 3819−3831.
(41) Brennan, M. C.; Kuno, M.; Rouvimov, S. Crystal Structure of Individual $CsPbBr_3$ Nanocubes. *Inorg. Chem.* **2019**, *58*, 1555−1560.
(42) Zhao, Q.; Hazarika, A.; Schelhas, L. T.; Liu, J.; Gaulding, A.; Li, G.; Zhang, M.; Toney, M. F.; Sercel, P. C.; Luther, J. M. Size-Dependent Lattice Structure and Confinement Properties in CsPbI3 Perovskite Nanocrystals: Negative Surface Energy for Stabilization. *ACS Energy Lett.* **2020**, *5*, 238−247.
(43) Akkerman, Q. A.; Abdelhady, A. L.; Manna, L. Zero-Dimensional Cesium Lead Halides: History, Properties, and Challenges. *J. Phys. Chem. Lett.* **2018**, *9*, 2326−2337.
(44) Li, J.; Yuan, X.; Jing, P.; Wei, M.; Hua, J.; Zhao, J.; Tian, L. Temperature-Dependent Photoluminescence of Inorganic Perovskite Nanocrystal Films. *RSC Adv.* **2016**, *6*, 78311.
(45) Yuan, X.; Hou, X.; Li, J.; Qu, C.; Zhang, W.; Zhao, J.; Li, H. Thermal Degradation of Luminescence in Inorganic Perovskite $CsPbBr_3$ Nanocrystals. *Phys. Chem. Chem. Phys.* **2017**, *19*, 8934.
(46) Bertolotti, F.; Protesescu, L.; Kovalenko, M. V.; Yakunin, S.; Cervellino, A.; Billinge, S. J.; Terban, M. W.; Pedersen, J. S.; Masciocchi, N.; Guagliardi, A. Coherent Nanotwins and Dynamic Disorder in Cesium Lead Halide Perovskite Nanocrystals. *ACS Nano* **2017**, *11*, 3819−3831.
(47) Paul, S.; Samanta, A. *N*-Bromosuccinimide as Bromide Precursor for Direct Synthesis and Highly Luminescent Green-Emitting Perovskite Nanocrystals. *ACS Energy Lett.* **2020**, *5*, 64.
(48) Yakunin, S.; Protesescu, L.; Krieg, F.; Bodnarchuk, M. I.; Nedelcu, G.; Humer, M.; De Luca, G.; Fiebig, M.; Heiss, W.; Kovalenko, M. V. Low-Threshold Amplified Spontaneous Emission and Lasing from Colloidal Nanocrystals of Caesium Lead Halide Perovskites. *Nat. Commun.* **2015**, *6*, 8056.
(49) Imran, M.; Caligiuri, V.; Wang, M.; Goldoni, L.; Prato, M.; Krahne, R.; De Trizio, L.; Manna, L. Benzoyl Halides as Alternative Precursors for the Colloidal Synthesis of Lead-Based Halide Perovskite Nanocrystals. *J. Am. Chem. Soc.* **2018**, *140*, 2656−2664.
(50) Pan, J.; Sarmah, S. P.; Murali, B.; Dursun, I.; Peng, W.; Parida, M. R.; Liu, J.; Sinatra, L.; Alyami, N.; Zhao, C.; Alarousu, E.; Ng, T. K.; Ooi, B. S.; Bakr, O. M.; Mohammed, O. F. Air-Stable Surface-Passivated Perovskite Quantum Dots for Ultra-Robust, Single- and Two-Photon-Induced Amplified Spontaneous Emission. *J. Phys. Chem. Lett.* **2015**, *6*, 5027−5033.
(51) Hirotsu, S.; Harada, J.; Iizumi, M.; Gesi, K. Structural Phase Transition in $CsPbBr_3$. *J. Phys. Soc. Jpn.* **1974**, *37*, 1393−1398.
(52) Verwey, J. F. Time and Intensity Dependence of the Photolysis of Lead Halides. *J. Phys. Chem. Solids* **1970**, *31*, 163−171.
(53) Albrecht, M. G.; Green, M. The Kinetics of the Photolysis of Thin Films of Lead Iodide. *J. Phys. Chem. Solids* **1977**, *38*, 297−306.
(54) Samu, G. F.; Balog, A.; De Angelis, F.; Meggiolaro, D.; Kamat, P. V.; Janaky, C. Electrochemical Hole Injection Selectively Expels Iodide from Mixed Halide Perovskite Films. *J. Am. Chem. Soc.* **2019**, *141*, 10812−10820.
(55) Motti, S. G.; Meggiolaro, D.; Barker, A. J.; Mosconi, E.; Perini, C. A. R.; Ball, J. M.; Gandini, M.; Kim, M.; De Angelis, F.; Petrozza, A. Controlling Competing Photochemical Reactions Stabilizes Perovskite Solar Cells. *Nat. Photonics* **2019**, *13*, 532−339.
(56) Park, J.-S.; Calbo, J.; Jung, Y.-K.; Whalley, L. D.; Walsh, A. Accumulation of Deep Traps at Grain Boundaries in Halide Perovskites. *ACS Energy Lett.* **2019**, *4*, 1321−1327.
(57) Chen, Q.; Zhou, H.; Song, T.-B.; Luo, S.; Hong, Z.; Duan, H.-S.; Dou, L.; Liu, Y.; Yang, Y. Controllable Self-Induced Passivation of Hybrid Lead Iodide Perovskites toward Hight Performance Solar Cells. *Nano Lett.* **2014**, *14*, 4158−4163.
(58) Kheraj, V.; Simonds, B. J.; Toshniwal, A.; Misra, S.; Peroncik, P.; Zhang, G.; Vardeny, Z. V.; Scarpulla, M. A. Using Photoluminescence to Monitor the Optoelectronic Properties of Methylammonium Lead Halide Perovskites in Light and Dark over Periods of Days. *J. Lumin.* **2018**, *194*, 353−358.
(59) Brenes, R.; Eames, C.; Bulovic, V.; Islam, M. S.; Stranks, S. D. The Impact of Atmosphere on the Local Luminescence Properties of Metal Halide Perovskite Grains. *Adv. Mater.* **2018**, *30*, 1706208.
(60) Brenes, R.; Guo, D.; Osherov, A.; Noel, N. K.; Eames, C.; Hutter, E. M.; Pathak, S. K.; Niroui, F.; Friend, R. H.; Islam, M. S.; Snaith, H. J.; Bulovic, V.; Savenije, T. J.; Stranks, S. D. Metal Halide Perovskite Polycrystalline Films Exhibiting Properties of Single Crystals. *Joule* **2017**, *1*, 155−167.
(61) Andaji-Garmaroudi, Z.; Anaya, M.; Pearson, A. J.; Stranks, S. D. Photobrightening in Lead Halide Perovskites: Observations, Mechanisms, and Future Potential. *Adv. Energy Mater.* **2020**, *10*, 1903109.
(62) Ravi, V. M.; Scheidt, R. A.; Nag, A.; Kuno, M.; Kamat, P. V. *To Exchange or Not to Exchange.* Suppressing Anion Exchange in Cesium Lead Halide Perovskites with $PbSO_4$-Oleate Capping. *ACS Energy Lett.* **2018**, *3*, 1049−1055.

https://dx.doi.org/10.1021/acsenergylett.0c00630
ACS Energy Lett. 2020, 5, 1465−1473